

## Supplementary information

### Textured interfaces in monolithic perovskite/silicon tandem solar cells: Advanced light management for improved efficiency and energy yield

Marko Jošt<sup>1\*</sup>, Eike Köhnen<sup>1</sup>, Anna Belen Morales-Vilches<sup>2</sup>, Benjamin Lipovšek<sup>3</sup>, Klaus Jäger<sup>4</sup>, Bart Macco<sup>5</sup>, Amran Al-Ashouri<sup>1</sup>, Janez Krč<sup>3</sup>, Lars Korte<sup>5</sup>, Bernd Rech<sup>5</sup>, Rutger Schlatmann<sup>2</sup>, Marko Topič<sup>3</sup>, Bernd Stannowski<sup>2</sup>, and Steve Albrecht<sup>1\*</sup>

<sup>1</sup>Young Investigator Group Perovskite Tandem Solar Cells, Helmholtz-Zentrum Berlin für Materialien und Energie GmbH, Kekuléstraße 5, 12489 Berlin, Germany

<sup>2</sup>PVcomB, Helmholtz Zentrum Berlin für Materialien und Energie, Schwarzschildstr. 3, 12489 Berlin, Germany

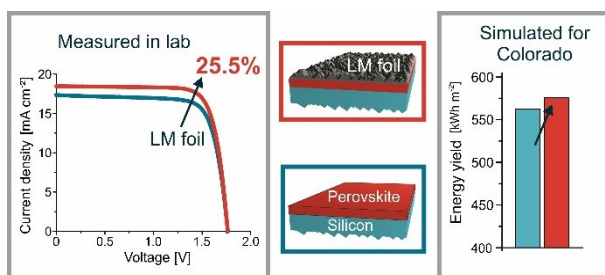
<sup>3</sup>University of Ljubljana, Faculty of Electrical Engineering, Tržaška 25, 1000 Ljubljana

<sup>4</sup>Young Investigator Group Nano-SIPPE, Helmholtz-Zentrum Berlin für Materialien und Energie GmbH, Albert-Einstein-Straße 16, 12489 Berlin, Germany

<sup>5</sup>Institute for Silicon Photovoltaics, Helmholtz-Zentrum Berlin für Materialien und Energie GmbH, Kekuléstraße 5, 12489 Berlin, Germany

(\* corresponding authors: [marko.jost@helmholtz-berlin.de](mailto:marko.jost@helmholtz-berlin.de), [steve.albrecht@helmholtz-berlin.de](mailto:steve.albrecht@helmholtz-berlin.de))

#### TOC

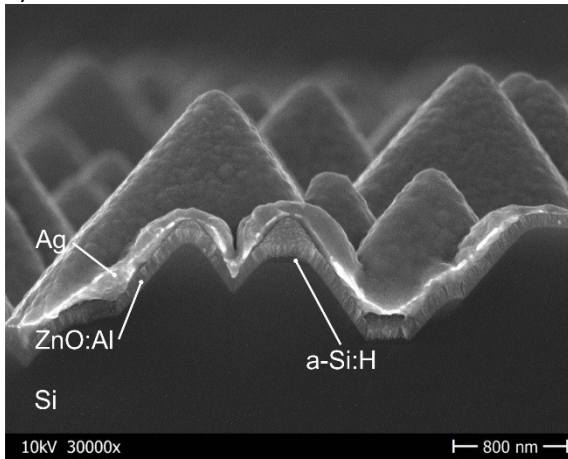


#### One sentence abstract

25.5% efficiency is demonstrated for monolithic perovskite/silicon tandem solar cell using textured foil and the impact of texture position on performance and energy yield is simulated.

## SEM cross-section of the silicon bottom cell

a)



b)

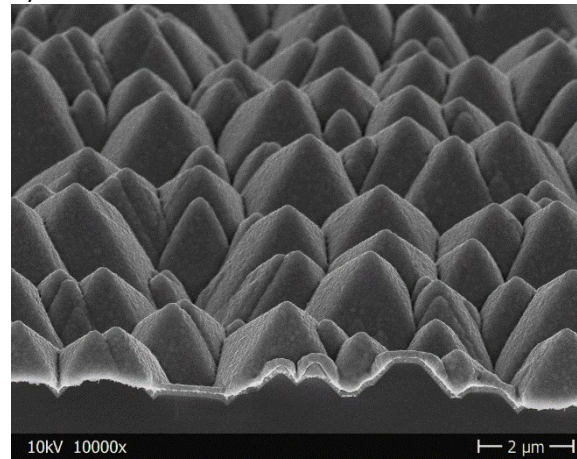


Figure S1: SEM cross-section image of the back-side of the silicon bottom cells used in tandem solar cell fabrication. SEM cross-section image of the back-side of the silicon bottom cells used in tandem solar cell fabrication. Image b) is recorded under tilt angle 30°.

## Comparison between JV measurements by using different illumination conditions

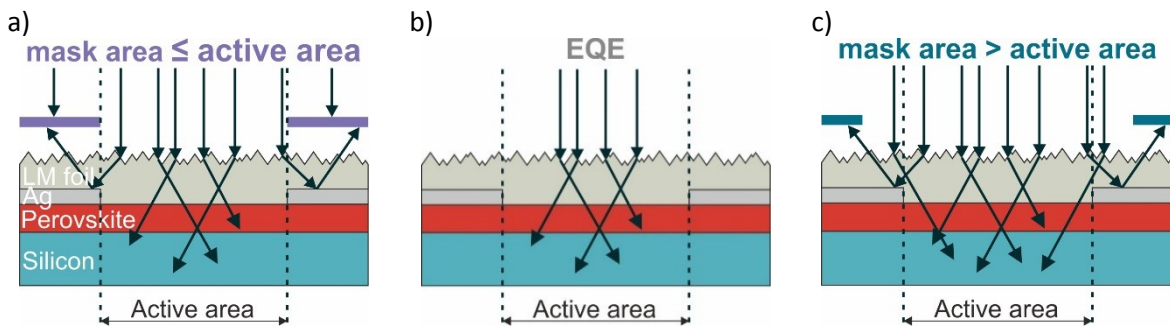


Figure S2: Schematic of measurements with different illumination conditions. a) With an aperture mask slightly smaller than the active area, some of the light that is initially in the active area is refracted outside. b) With the small spot EQE all of the light stays within the active area. c) With an aperture mask larger than the active area, some of the light from inside the active area is scattered out but some of the light from outside the active area is refracted back in. This value serves as the potential tandem efficiency when being integrated into a module with glass encapsulation.

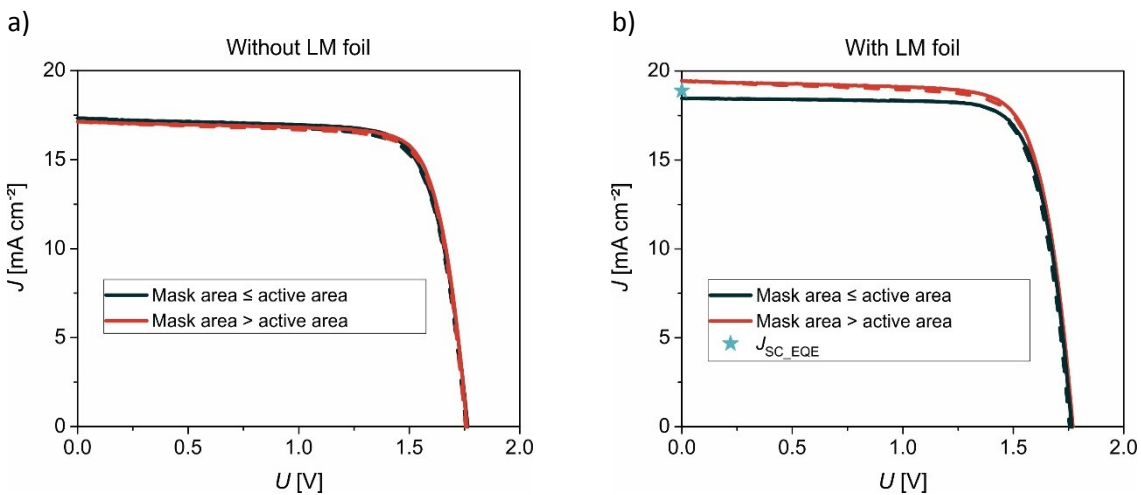


Figure S3: Comparison between JV measurements by using different illumination conditions. a) Measurements without the light management (LM) foil and b) measurements with the LM foil. Black lines represent illumination conditions with the aperture mask being slightly smaller than the active area, and red lines with the aperture mask being larger than the active area. Dashed lines are forward scans, solid lines reverse scans. The blue star represents  $J_{sc}$  calculated from the EQE spectra of the limiting sub-cell, here silicon.

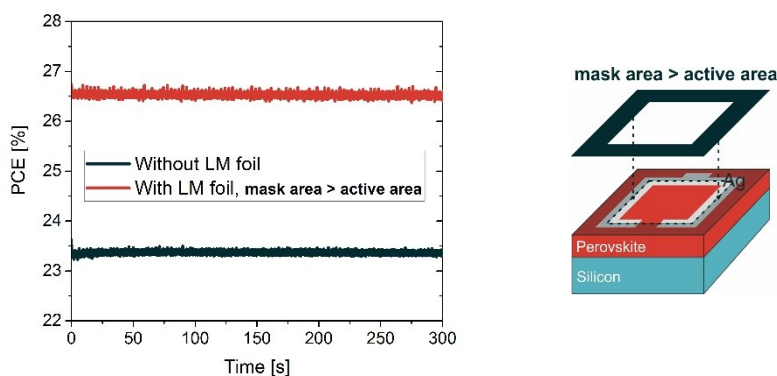


Figure S4: MPP tracking over 5 min of the fabricated tandem device without (black) and with (red) the LM foil, measured with mask area  $>$  active area as shown on the right side and in Figure S1. The values are stable over 5 min MPP tracking and very close to the respective JV scans, see Table 1 in the main paper.

## Origin of the $(n,k)$ spectra

Table S1: List of refractive indices  $(n, k)$ , method of determination and source.

Material/Layer	Method	Source
LM foil	reflectance / transmittance	[1]
LiF	spectral ellipsometry	[2]
IZO	spectral ellipsometry	This work
SnO <sub>2</sub>	spectral ellipsometry	This work
C60	spectral ellipsometry	[3]
Perovskite	Adapted from literature	[4]
PTAA	spectral ellipsometry	[1]
ITO	spectral ellipsometry	[3]
nc-SiO <sub>x</sub> :H	spectral ellipsometry	[3]
a-Si:H (i)	reflectance / transmittance	[2]
Silicon	Adapted from literature	PV Lighthouse [5]
a-Si:H (i)	reflectance / transmittance	[2]
a-Si:H (p <sup>+</sup> )	reflectance / transmittance	[2]
ZnO:Al	spectral ellipsometry	[3]
Ag	Adapted from literature	PV Lighthouse [5]

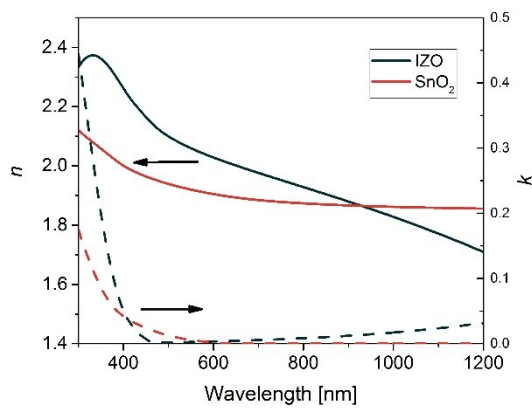


Figure S5: The  $(n, k)$  data for IZO (black) and SnO<sub>2</sub> (red) obtained for this work.

## Matching between simulations and experiment

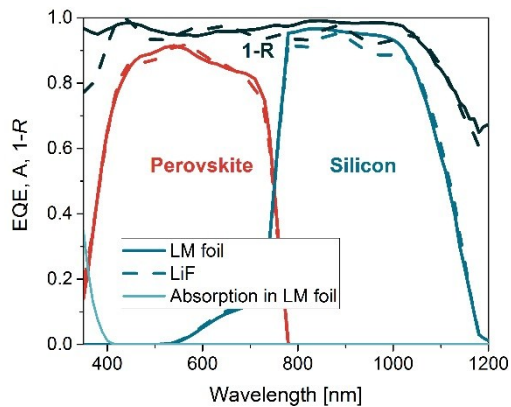
Table S2: Layers in the tandem device stack and their thicknesses used in the simulating the fabricated device. A perovskite band-gap with 1.60 eV was used. The implied  $J_{SC\_SIM}$  of each layer is also shown for the two simulation cases – with and without the LM foil.

Layer	Thickness [nm]	$J_{SC\_sim}$ [mA cm <sup>-2</sup> ]		Change [mA cm <sup>-2</sup> ]
		Without LM foil	With LM foil	
LM foil/glass	100000/200000		0.16	
IZO	122	1.60	1.94	
SnO <sub>2</sub>	20	0.10	0.11	
C60	12	0.56	0.64	
Perovskite	<b>560</b>	<b>17.29</b>	<b>19.84</b>	<b>2.55</b>
PTAA	10	0.01	0.01	
ITO	20	0.24	0.25	
nc-SiO <sub>x</sub> :H	95	0.01	0.01	
a-Si:H (i)	5	0.01	0.01	
Silicon	<b>250000</b>	<b>18.59</b>	<b>19.60</b>	<b>1.01</b>
a-Si:H (i)	5	0.00	0.00	
a-Si:H (p <sup>+</sup> )	8	0.00	0.00	
ZnO:Al	70	0.57	0.57	
Ag	500	0.64	0.65	
Reflection		<b>6.61</b>	<b>2.41</b>	<b>-4.20</b>

## Comparison of the textured LM foil with the planar LiF AR coating applied on top of the fabricated device

For the fabricated device, a larger improvement with the LM foil compared to the LiF AR coating is observed, especially in the silicon-absorbing wavelength range. When the device is not fully optically optimized the LM foil effect is greater than from the planar AR coating. The reduced reflection in the UV wavelength range (at 350 nm) with LM foil is not directly translated into current due to absorption in the LM foil itself in the UV (UV light is needed to cure the polymer and is thus partially absorbed).

a)



b)

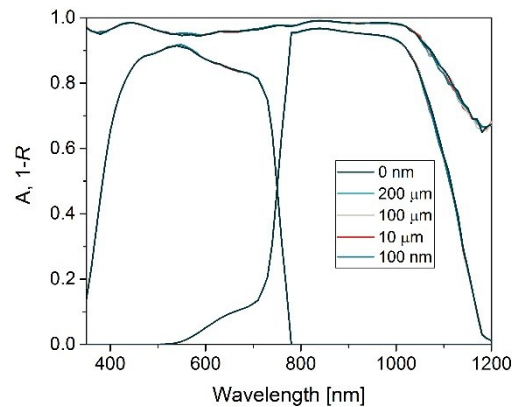


Figure S6: a) Simulated absorptance and reflectance (plotted as 1-R) spectra for tandem devices with either textured front side LM foil (solid) or planar antireflective coating made from a LiF layer atop the front TCO (dashed). Perovskite spectra are red, silicon black and 1-R blue. The absorption in the LM foil is also shown as a solid light blue line. b) Simulated absorptance and reflectance (plotted as 1-R) spectra for tandem devices with textured LM foil and different thickness of index matching liquid as indicated in the legend.

## Optimization of the flat tandem device (A)

Table S3: Simulated optimal layer thicknesses and the corresponding performance metrics of a flat tandem solar cell (Device A) stack for different perovskite bandgaps. The first column describes the layers. The second and the third columns contain the experimentally relevant minimum and maximum layer thicknesses used as boundary conditions in optical optimization. The thicknesses of the layers in the bottom cell were fixed and only the layers above the silicon substrate were varied in thickness. Other columns show optimal thicknesses of the layer optimized for different perovskite bandgaps. The last column shows the selected thicknesses that were later used for further optimization. All values are in nm. Bottom part of the table shows resulting  $J_{SC}$  and PCE values assuming  $FF = 80\%$  and  $V_{OC} = 710 \text{ mV} + E_{g\_perovskite}/q - 400 \text{ mV}$ .

Layer	Min thickness	Max thickness	Eg 1.56 eV	Eg 1.60 eV	Eg 1.64 eV	Eg 1.69 eV	Eg 1.73 eV	Selected
LiF	80	130	106	109	107	106	103	105
IZO	80	150	80	82	80	80	80	80
SnO <sub>2</sub>	10	20	10	10	10	10	10	10
C <sub>60</sub>	10	20	10	10	10	10	10	10
Pero	0	2500	325	430	585	1008	2415	800-1200
PTAA	5	15	13	9	14	13	6	10
ITO	20	40	21	27	20	20	33	20
nc-SiO <sub>x</sub>	20	150	100	97	96	95	54	95
Pero $J_{SC\_SIM}$ [mAcm <sup>-2</sup> ]			19	18.99	19.07	19.12	18.73	
cSi $J_{SC\_SIM}$ [mAcm <sup>-2</sup> ]			18.99	18.98	19.07	19.11	18.7	
$J_{SC\_SIM}$ [mAcm <sup>-2</sup> ]			18.99	18.98	19.07	19.11	18.7	
FF [%]			80	80	80	80	80	
V <sub>OC</sub> [V]			1.87	1.91	1.95	2.00	2.04	
PCE [%]			28.4	29.0	29.8	30.5	30.6	

Table S4: As electrical performance strongly varies with the charge selective contact thickness, we have considered in our simulations only thicknesses of SnO<sub>2</sub>, C60 and PTAA contact within lower and upper bounds, or selective layers that yield high performance without being limited by the contact itself. The table also presents references to where these results were experimentally realized.

Layer	Lower bound	Upper bound	This work
SnO <sub>2</sub>	7 nm [6]	20 nm [7]	20 nm
C60	1 nm [8]	20 nm [9], [10]	12 nm
PTAA	5 nm [11]	50 nm doped [12]	10 nm

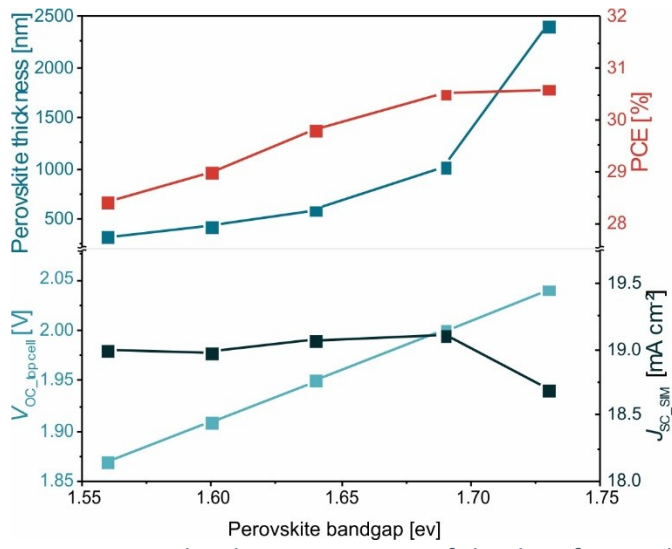
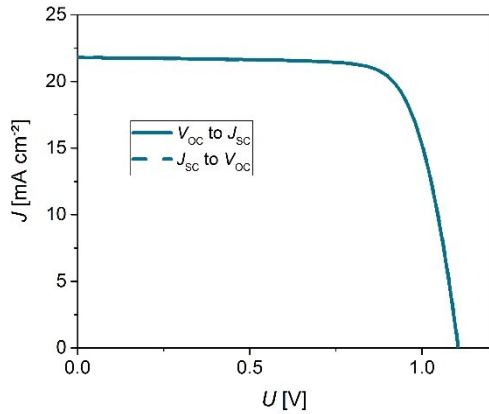


Figure S7: Graphical representation of the data from Table S3 where flat tandem solar cell (Device A) was optimized for highest PCE for different bandgaps.

Reference single-junction solar cell with 800 nm thick perovskite absorber layer

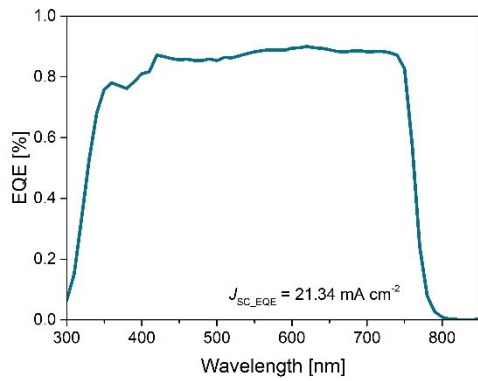
a)



b)

	$J_{sc}$ [mA cm <sup>-2</sup> ]	$V_{oc}$ [V]	FF [%]	PCE [%]
forward	21.8	1.11	76.3	18.4
reverse	21.8	1.11	76.3	18.4

c)



d)

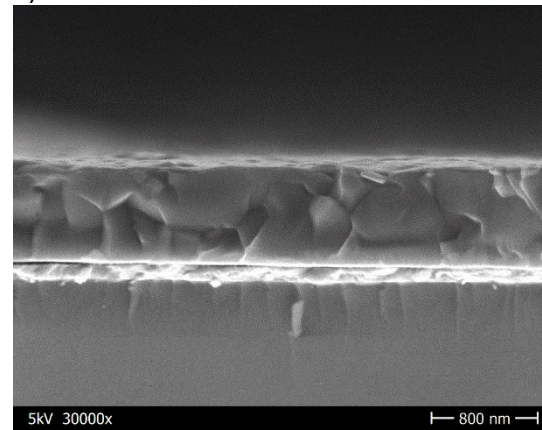


Figure S8: a) J-V characteristics, b) PV parameters, c) EQE spectra and d) SEM cross-section image of a single junction device with 800 nm thick perovskite absorber, showing that efficient devices with thick (~800 nm) perovskite films can be fabricated. The layer configuration of the device is glass/ITO/PTAA/perovskite/C60/BCP/Ag thus this is an equivalent single-junction opaque reference device for the fabricated tandem device, however, with thicker active layer.

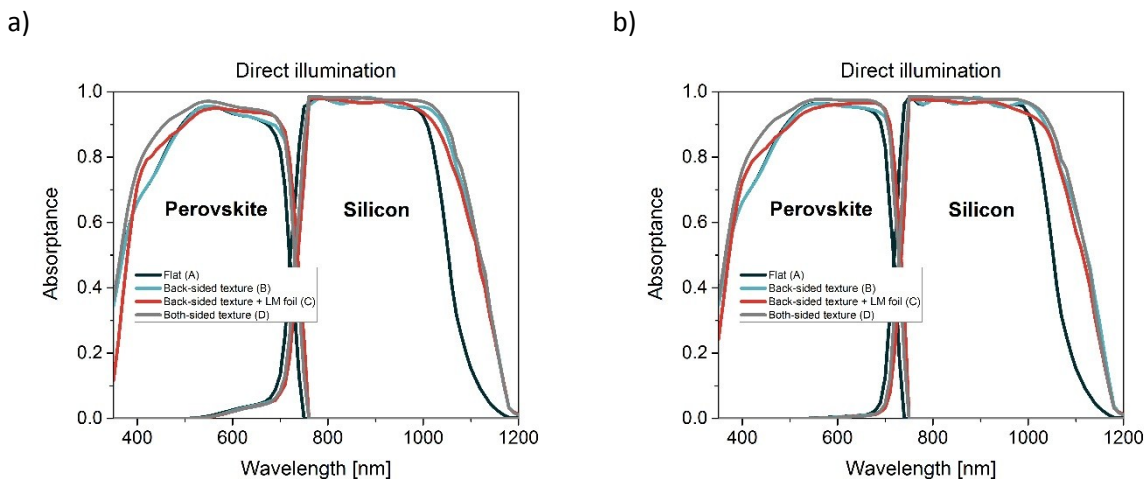
## Optical simulations for perovskite thicknesses of 800 nm and 1200 nm

Table S5 and Figure S9 show the simulations with perovskite thicknesses of 800 nm and 1200 nm. We observe that with increasing the perovskite thickness, the optimal bandgap also increases. Interestingly, the predicted efficiency of a 200 nm thicker perovskite layer (1200 nm) is only 0.1% absolute higher than the one of a 1000 nm layer. The small increase can be explained by comparing the absorption spectra in Figure 5a and Figure S9. The main change is the reduction of silicon contribution in the region between 550 and 800 nm where perovskite and silicon absorption overlap. Once this overlap is exhausted, no extra current can be generated in perovskite by increasing its thickness. The improvement with a significantly thicker perovskite would therefore only be minimal.

Comparing the ideal case with no perovskite thickness or bandgap constraints (see Table S2), we see that the efficiency for the device (A) would only be 0.1% absolute higher, however, the perovskite would have to be 1400 nm thicker with a bandgap of 1.73 eV. This justifies the fixing of perovskite thickness and only tuning the bandgap.

*Table S5: Simulated photovoltaic performance parameters for designs (A), (B), (C) and (D) and fixed perovskite thicknesses (800, 1000 and 1200 nm). Indicated is the optimal perovskite bandgap for each simulated device design,  $J_{SC\_SIM}$ ,  $V_{OC}$ , FF and PCE.  $V_{OC} = 710 \text{ mV} + E_{g\_perovskite}/q - 400 \text{ mV}$ .*

	Perovskite thickness [nm]	$E_g$ [eV]	$J_{SC\_SIM}$ [ $\text{mA cm}^{-2}$ ]	$V_{OC}$ [V]	FF [%]	PCE [%]
<b>Flat (A)</b>	800	1.68	18.98	1.99	80	30.2
	1000	1.69	19.07	2.00	80	30.5
	1200	1.70	19.03	2.01	80	30.6
<b>Back texture (B)</b>	800	1.64	19.88	1.95	80	31.1
	1000	1.65	20.01	1.96	80	31.4
	1200	1.66	19.94	1.97	80	31.5
<b>BackT + LM foil (C)</b>	800	1.64	20.04	1.95	80	31.3
	1000	1.66	19.97	1.97	80	31.5
	1200	1.66	20.05	1.97	80	31.7
<b>Double texture (D)</b>	800	1.65	20.50	1.96	80	32.2
	1000	1.66	20.56	1.97	80	32.5
	1200	1.68	20.50	1.99	80	32.6



*Figure S9: Simulated EQE and spectra for the different device configurations (A), (B), (C) and (D) where only direct illumination is considered for perovskite thickness of a) 800 nm and b) 1200 nm.*

## Loss analysis

Absorbance profiles of the simulated fabricated device with the LM foil (design C, but fabricated device and not optically optimized) and the best simulated design, both-side textured device (D) with 1000 nm thick perovskite is shown in Figure S10 while Figure S11 shows direct comparison between the photocurrent density utilization and losses of both considered cases. A much better utilization of the perovskite and silicon photocurrent in the optimal device (D) can be observed; the absolute photocurrent density yield is  $1.92 \text{ mA cm}^{-2}$  lower in the fabricated device. The overlap between perovskite and silicon is almost exhausted. Additionally, despite the significant reduction of reflection with the LM foil, the reflection of the device (D) is still much lower; the reflection losses are  $1.1 \text{ mA cm}^{-2}$  lower in the optimized device. Thinner IZO layer (122 nm in the experiment and 80 nm in best simulation of device (D)) helps to reduce the losses by  $0.6 \text{ mA cm}^{-2}$ . The other losses are almost the same. This further confirms that our layer stack is optically good, the only improvement could be with a thinner IZO. However, the series resistance might increase. The  $J_{SC\_SIM}$  values of all the layers are shown in Table S6 with absolute values.

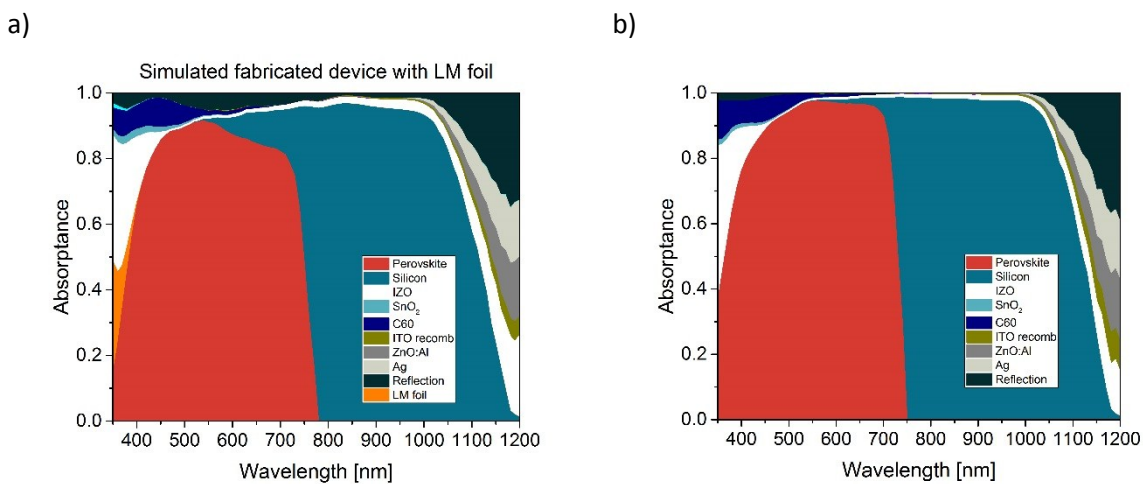


Figure S10: Absorption profiles for a) simulated fabricated device with the LM foil and b) the best simulated case, both-side textured device (D) with a 1000 nm thick perovskite. The simulated short-circuit current densities are shown in Table S6.

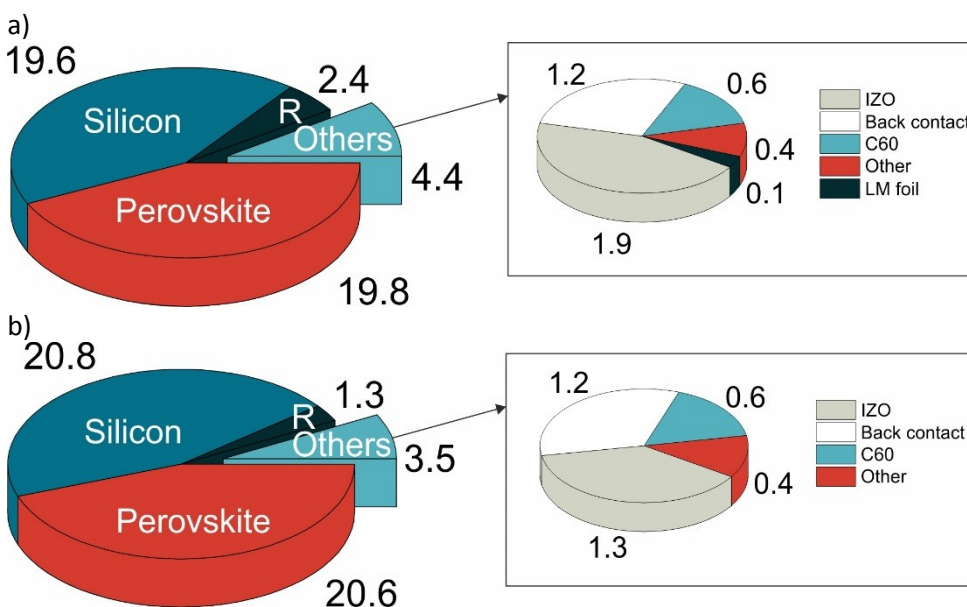


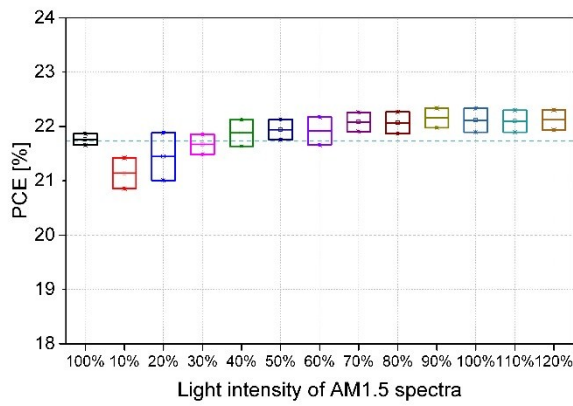
Figure S11: The loss comparison between a) simulated fabricated device with the LM foil (blue) and b) the best simulated both-side textured device (D) with a 1000 nm thick perovskite (red). All values are in  $\text{mA cm}^{-2}$ .

Table S6: Simulated absorption and loss analysis for a both-side textured tandem device (D) with a 1000 nm thick perovskite and fabricated device with the LM foil (this data is repeated from Table S2 for easier comparison).

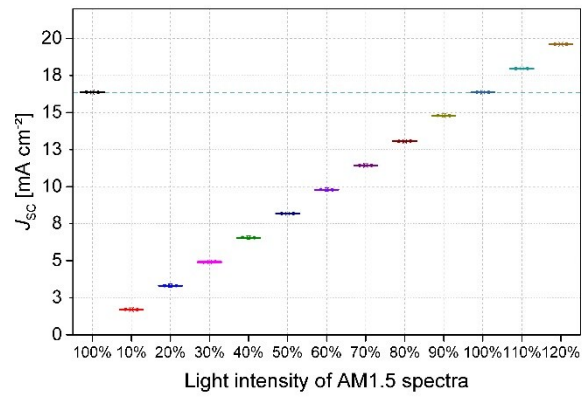
Device (D) (1000 nm thick perovskite)		Device (C) experiment (560 nm thick perovskite)	
Layer	Absorption/reflection [mA cm <sup>-2</sup> ]	Layer	Absorption/reflection [mA cm <sup>-2</sup> ]
<b>Reflection</b>	<b>1.34</b>	<b>Reflection</b>	<b>2.41</b>
LiF	0	LM foil/glass	0.16
IZO	1.34	IZO	1.94
SnO <sub>2</sub>	0.06	SnO <sub>2</sub>	0.11
C <sub>60</sub>	0.59	C60	0.64
<b>Perovskite</b>	<b>20.56</b>	<b>Perovskite</b>	<b>19.84</b>
PTAA	0.01	PTAA	0.01
ITO	0.35	ITO	0.25
nc-SiO <sub>x</sub> :H	0.00	nc-SiO <sub>x</sub> :H	0.01
a-Si:H (i)	0.00	a-Si:H (i)	0.01
<b>Silicon</b>	<b>20.80</b>	<b>Silicon</b>	<b>19.60</b>
a-Si:H (i)	0	a-Si:H (i)	0.00
a-Si:H (p <sup>+</sup> )	0	a-Si:H (p <sup>+</sup> )	0.00
ZnO:Al	0.55	ZnO:Al	0.57
Ag	0.63	Ag	0.65

*JV* measurements under different light intensities- fabricated tandem device without LM foil

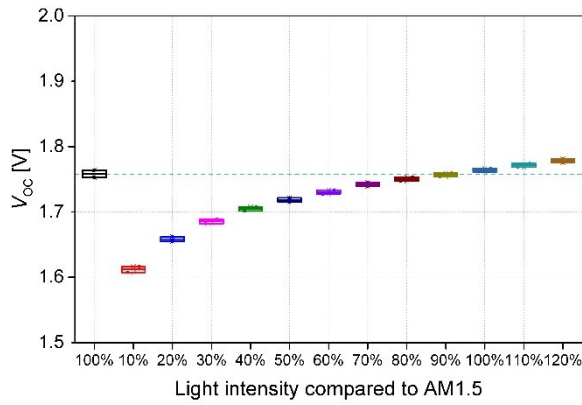
a)



b)



c)



d)

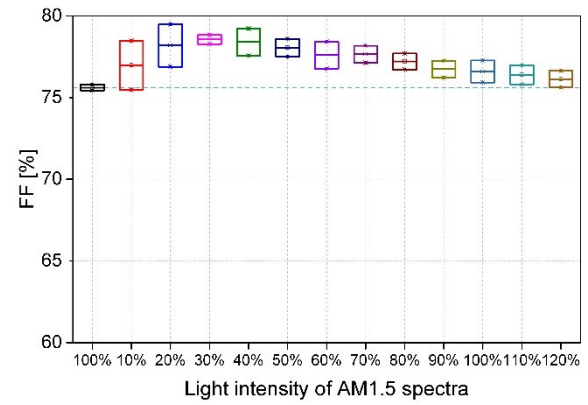


Figure S12: Experimentally measured photovoltaic parameters, a) PCE, b)  $J_{sc}$ , c)  $V_{oc}$  and d) FF for different light intensities for a tandem cell without LM foil displayed in intensity of one sun. 100% means the intensity of the calibrated AM 1.5G spectra of the LED based sun simulator, 10% means that the intensity is reduced to a tenth of the calibrated AM 1.5G spectra. Forward and reverse measurements and their average are shown in each box.

## Energy yield

The position of the Sun in the sky is defined by a zenith and azimuth angle. Figure S13 shows the photocurrent dependency on the zenith angle at a fixed azimuth angle. The integrated absorption spectra over the solar spectrum (AM1.5 in this case) exhibit cosine dependency, influenced by cosine angle dependency on the incident illumination. Overall, the relative improvements compared to device (A) are constant. However, for the larger zenith angles (>50°) a clear improvement with the front-side texture is exhibited due to more advantageous incidence angle upon a pyramid compared to a flat surface.

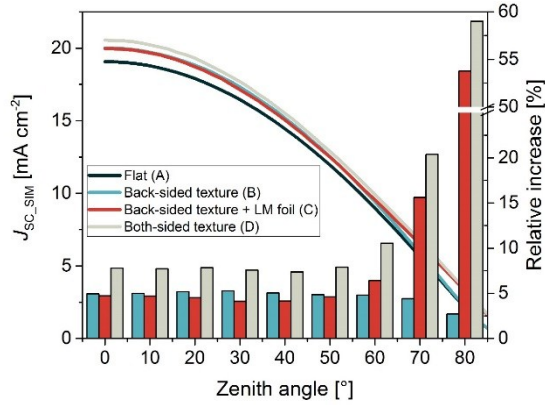


Figure S13: a) Simulated photocurrent  $J_{SC\_SIM}$  in dependence of zenith angle at a fixed azimuth angle for the optimized four designs. Perovskite with thickness of 1000 nm was chosen. Relative increase compared to the design (A) is shown with a bar graph and the legend on the right side.

However, when calculating the energy yield, we took the zenith ( $\theta$ ) and azimuth ( $\varphi$ ) angles of the sun (and the tilt of the solar cell) into the account.

$$J_{sc\_pero} = \frac{q}{h * c} \int_{300\text{ nm}}^{1200\text{ nm}} [A_{diff\_pero}(\lambda) * DHI'(\lambda, t) + A_{dir\_pero}(\theta, \varphi, \lambda) * DNI'(\lambda, t)] \lambda d\lambda \quad 1$$

$$J_{sc\_Si} = \frac{q}{h * c} \int_{300\text{ nm}}^{1200\text{ nm}} [A_{diff\_Si}(\lambda) * DHI'(\lambda, t) + A_{dir\_Si}(\theta, \varphi, \lambda) * DNI'(\lambda, t)] \lambda d\lambda \quad 2$$

$$W = \int_{year} \min(J_{sc\_pero}(t), J_{sc\_Si}(t)) * V_{OC}(E(\alpha, t)) * FF(E(\alpha, t)) dt \quad 3$$

$$DHI' = GHI - DNI * \cos(\theta, \varphi) \quad 4$$

$$DNI' = DNI * \cos(\theta, \varphi) \quad 5$$

We calculate yearly energy yield by using equation 1, 2 and 3; since we focus on the optical point of view, we neglect the temperature effect. Equations 1 and 2 are used to determine the photocurrent of each subcell, where  $\lambda$  is wavelength,  $q$  is elementary charge and  $h$  is Planck's constant.  $A_{diff}$  and  $A_{dir}$  are absorption spectra of a device under diffuse and direct illumination, respectively. DHI, DNI and GHI denote diffuse horizontal irradiance, direct normal irradiance and global horizontal irradiance, respectively; DNI and GHI are obtained from NREL in an hourly interval [13].  $DNI * \cos(\theta, \varphi)$  denotes the projection of the direct light on the normal of the device.  $J_{SC}$  is then calculated by superposition of diffuse and direct  $J_{SC\_SIM}$  contribution, and the minimum of  $J_{SC\_pero}$  and  $J_{SC\_Si}$  is used. The dependency of  $V_{OC}$  and  $FF$  on light intensity  $E$  were chosen as described in the main text.



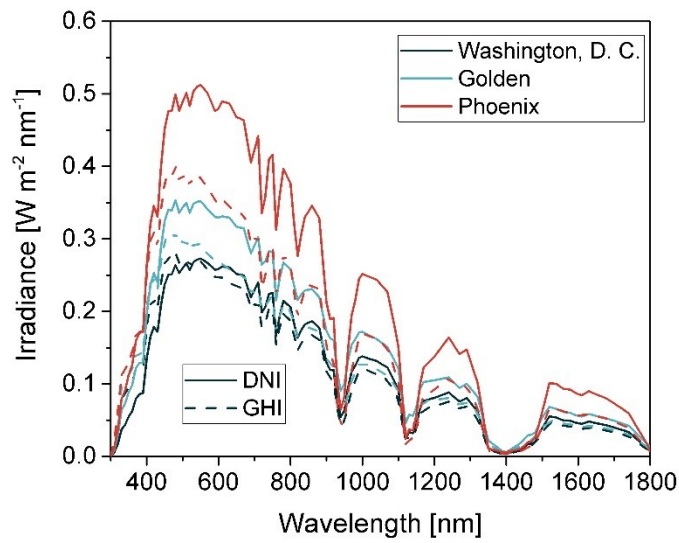
Table S7: Estimated energy yield based on the simulation for all the considered different tandem device design cases for three locations: Washington, Golden and Phoenix when the solar cell is either at 30° or 90° angle with respect to the ground. The 30° angle would represent a solar module in typical solar farms whereas the 90° value would more likely be relevant for building integrated photovoltaics (BIPV).

		<b>Flat (A)</b>		<b>Back-textured (B)</b>		<b>Back-textured + LM foil (C)</b>		<b>Both-side texture (D)</b>	
		Total [kWh m <sup>-2</sup> ]	Rel. inc. vs (A) [%]	Total [kWh m <sup>-2</sup> ]	Rel. inc. vs (A) [%]	Total [kWh m <sup>-2</sup> ]	Rel. inc. vs (A) [%]	Total [kWh m <sup>-2</sup> ]	Rel. inc. vs (A) [%]
<b>30°</b>	<b>Washington</b>	485.8	0	500.1	3.0	512.3	5.5	534.2	10.0
	<b>Golden</b>	544.1	0	562.2	3.3	575.5	5.8	595.3	9.4
	<b>Phoenix</b>	662.6	0	679.7	2.6	694.7	4.8	725.6	9.5
<b>90°</b>	<b>Washington</b>	346.4	0	355.9	2.7	371.7	7.3	389.9	12.6
	<b>Golden</b>	382.1	0	394.1	3.2	410.9	7.6	425.2	11.3
	<b>Phoenix</b>	363.2	0	371.1	2.2	392.8	8.1	416.3	14.6

Table S8: Yearly direct, diffuse and total irradiance for the three locations calculated from the typical meteorological year (TMY).

<b>Yearly irradiance</b>	<b>Direct [kWh m<sup>-2</sup>]</b>	<b>Diffuse [kWh m<sup>-2</sup>]</b>	<b>Total [kWh m<sup>-2</sup>]</b>
<b>Washington</b>	894.00	497.38	1391.37
<b>Golden</b>	1107.98	453.40	1561.38
<b>Phoenix</b>	1607.04	310.54	1917.59

a)



b)

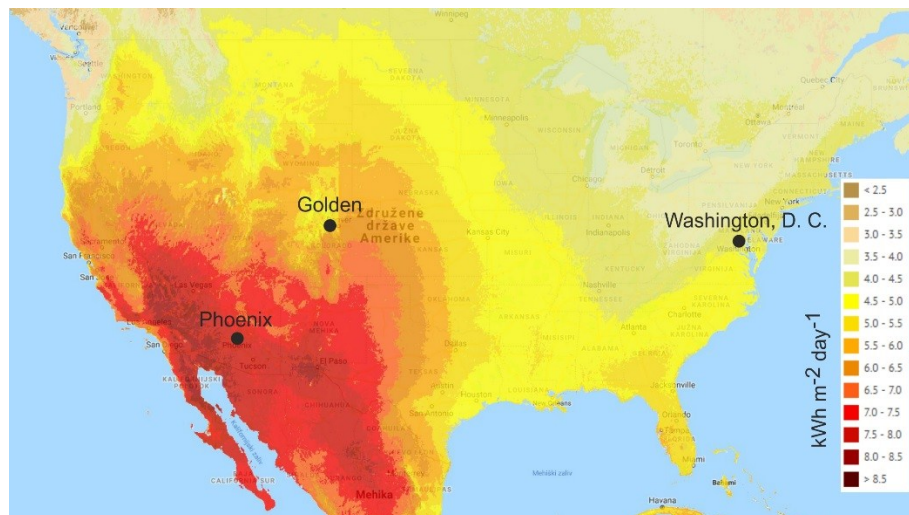


Figure S14: A) Spectral irradiance as function of wavelength averaged over a year as obtained from NREL for the three compared locations: Golden (black), Phoenix (blue) and Washington, D. C. (red). Shown are the GHI and DNI spectra which represent the Global Horizontal Irradiance and Direct Normal Irradiance, respectively. Solid lines represent DNI and dashed GHI. B) Yearly sun irradiance map with denoted locations, obtained from NREL.

## References

- [1] M. Jošt *et al.*, "Efficient Light Management by Textured Nanoimprinted Layers for Perovskite Solar Cells," *ACS Photonics*, vol. 4, no. 5, pp. 1232–1239, May 2017.
- [2] K. Jäger, L. Korte, B. Rech, and S. Albrecht, "Numerical optical optimization of monolithic planar perovskite-silicon tandem solar cells with regular and inverted device architectures," *Opt. Express*, vol. 25, no. 12, pp. A473–A482, Jun. 2017.
- [3] L. Mazzarella *et al.*, "Infrared photocurrent management in monolithic perovskite/silicon heterojunction tandem solar cells by using a nanocrystalline silicon oxide interlayer," *Opt. Express*, vol. 26, no. 10, pp. A487–A497, May 2018.
- [4] P. Löper *et al.*, "Complex Refractive Index Spectra of CH<sub>3</sub>NH<sub>3</sub>PbI<sub>3</sub> Perovskite Thin Films Determined by Spectroscopic Ellipsometry and Spectrophotometry," *J. Phys. Chem. Lett.*, vol. 6, no. 1, pp. 66–71, Jan. 2015.
- [5] "PV Lighthouse." [Online]. Available: <https://www.pvlighthouse.com.au/>. [Accessed: 18-Jul-2018].
- [6] K. A. Bush *et al.*, "23.6%-efficient monolithic perovskite/silicon tandem solar cells with improved stability," *Nat. Energy*, vol. 2, no. 4, p. 17009, Apr. 2017.
- [7] K. O. Brinkmann *et al.*, "Suppressed decomposition of organometal halide perovskites by impermeable electron-extraction layers in inverted solar cells," *Nat. Commun.*, vol. 8, p. 13938, Jan. 2017.
- [8] D. Liu *et al.*, "Impact of Ultrathin C60 on Perovskite Photovoltaic Devices," *ACS Nano*, vol. 12, no. 1, pp. 876–883, Jan. 2018.
- [9] A. Magomedov *et al.*, "Self-Assembled Hole Transporting Monolayer for Highly Efficient Perovskite Solar Cells," *Adv. Energy Mater.*, vol. 0, no. 0, p. 1801892.
- [10] Z. Xiao *et al.*, "Unraveling the hidden function of a stabilizer in a precursor in improving hybrid perovskite film morphology for high efficiency solar cells," *Energy Environ. Sci.*, vol. 9, no. 3, pp. 867–872, Mar. 2016.
- [11] M. Stollerfoht *et al.*, "Approaching the Fill Factor Shockley Queisser Limit in Stable, Dopant-Free Triple Cation Perovskite Solar Cells," *Energy Environ. Sci.*, May 2017.
- [12] Q. Han *et al.*, "High-performance perovskite/Cu(In,Ga)Se<sub>2</sub> monolithic tandem solar cells," *Science*, vol. 361, no. 6405, pp. 904–908, Aug. 2018.
- [13] "NSRDB Viewer | National Solar Radiation Database (NSRDB)." [Online]. Available: <https://nsrdb.nrel.gov/nsrdb-viewer>. [Accessed: 07-Jul-2018].